



**METHODS AND APPROACHES**

# A four-electrode method to study dynamics of ion activity and transport in skeletal muscle fibers

 Judith A. Heiny<sup>1</sup>, Stephen C. Cannon<sup>2</sup> , and Marino DiFranco<sup>2</sup> 

**Ion movements across biological membranes, driven by electrochemical gradients or active transport mechanisms, control essential cell functions. Membrane ion movements can manifest as electrogenic currents or electroneutral fluxes, and either process can alter the extracellular and/or intracellular concentration of the transported ions. Classic electrophysiological methods allow accurate measurement of membrane ion movements when the transport mechanism produces a net ionic current; however, they cannot directly measure electroneutral fluxes and do not detect any accompanying change in intracellular ion concentrations. Here, we developed a method for simultaneously measuring ion movements and the accompanying dynamic changes in intracellular ion concentrations in intact skeletal muscle fibers under voltage or current clamp in real time. The method combines a two-microelectrode voltage clamp with ion-selective and reference microelectrodes (four-electrode system). We validate the electrical stability of the system and the viability of the preparation for periods of ~1 h. We demonstrate the power of this method with measurements of intracellular Cl<sup>-</sup>, H<sup>+</sup>, and Na<sup>+</sup> to show (a) voltage-dependent redistribution of Cl<sup>-</sup> ions; (b) intracellular pH changes induced by changes in extracellular pCO<sub>2</sub>; and (c) electroneutral and electrogenic Na<sup>+</sup> movements controlled by the Na,K-ATPase. The method is useful for studying a range of transport mechanisms in many cell types, particularly when the transmembrane ion movements are electrically silent and/or when the transport activity measurably changes the intracellular activity of a transported ion.**

## Introduction

Ion movements across biological membranes control essential cell functions. A wide range of electrophysiological approaches exist to measure ion movements by membrane channels and pumps with good sensitivity and time resolution. However, not all biologically important membrane transport processes can be studied using these approaches. Existing electrophysiological techniques detect transmembrane ion movements only when the transport mechanism produces a net change in membrane potential (e.g., transport by ion channels or electrogenic pumps) or a net charge transfer across the membrane. Consequently, they do not detect electroneutral transport processes (carriers, exchangers, etc.). In addition, it is often the change in intracellular concentration of a transported ion that determines the cellular response. However, this dynamic information is lost when the intracellular concentration is measured under steady-state conditions at an end point of the measurement, as is commonly done.

Here, we describe a method to simultaneously measure transmembrane ion movements and the accompanying

transient changes in intracellular ion concentration (or, more importantly, changes in ion activity). The activity of an ion, rather than the total (bound + free) concentration, is important because it determines the membrane potential, equilibrium potentials, and other parameters that determine the cellular response (Tsien, 1989).

Ion-selective microelectrodes (ISMs), in particular liquid membrane ISMs, represent a highly-sensitive method for measuring the intracellular activity of physiologically relevant ions (Kessler et al., 1976; Armstrong and Garcia-Diaz, 1980; Mooney et al., 1988). An ISM is constructed by filling the tip of a silanized glass micropipette with a water-immiscible organic phase doped with a specific lipophilic ionophore, and filling the rest of the micropipette with saline containing the ion of interest. When in contact with an aqueous media (e.g., a solution, the cytoplasm) containing the ion of interest, a voltage is generated across the organic phase ( $V_{ion}$ ) which typically shows a Nernstian dependence on ion activity. When impaled in a cell, the voltage

<sup>1</sup>Department of Pharmacology and Systems Physiology, University of Cincinnati, Cincinnati, OH; <sup>2</sup>Department of Physiology, David Geffen School of Medicine at University of California, Los Angeles, Los Angeles, CA.

Correspondence to Marino DiFranco: [mdifranco@mednet.ucla.edu](mailto:mdifranco@mednet.ucla.edu)

A preliminary abstract of this work has been published (Heiny, J.A., S.C. Cannon, and M. DiFranco. 2018. A four microelectrode method to study intracellular ion concentration and transport in skeletal muscle fibers. *Biophysical Journal*, Vol. 114, Abstr. 627a).

© 2019 Heiny et al. This article is distributed under the terms of an Attribution–Noncommercial–Share Alike–No Mirror Sites license for the first six months after the publication date (see <http://www.rupress.org/terms/>). After six months it is available under a Creative Commons License (Attribution–Noncommercial–Share Alike 4.0 International license, as described at <https://creativecommons.org/licenses/by-nc-sa/4.0/>).

readout of an ISM ( $V_{ISM}$ ) equals the arithmetic sum of  $V_{ion}$  and the membrane potential ( $V_m$ ;  $V_{ISM} = V_{ion} + V_m$ ). Thus, to obtain  $V_{ion}$ ,  $V_m$  must be measured, ideally from the same position in the cell.

The most common practical implementations of ISMs entail the use of single- or double-barrel micropipettes. For single-barrel ISMs,  $V_m$  is measured with a second independent (sharp) microelectrode, while for double-barrel ISMs, one channel is filled with an appropriate aqueous saline and used to measure  $V_m$ . An obvious advantage of double-barrel ISMs is that only one impalement is required. However, their fabrication is somewhat cumbersome. Single-barrel ISMs are easier to fabricate, but more skill and instrumentation is required to impale a cell with two microelectrodes. With multicellular preparations, it is necessary to confirm that both electrodes are inside the same cell by passing bridge-corrected current pulses through the reference electrode. Configurations such as these are commonly used to measure (“normal” or “physiological”) ion activities in preparations maintained at physiological conditions, or even in live animals (Zeuthen and Monge, 1975). These approaches have inherent limitations. Membrane damage due to impalement of double-barrel electrodes or two single-barrel electrodes causes membrane depolarization (Kessler et al., 1976; Koryta and Stulik, 1983; Mooney et al., 1988) which, as demonstrated below, can cause voltage-dependent redistribution of ions of interest. In general, it is not possible to maintain a fixed membrane potential by passing current through the reference electrode, because this can produce spurious voltage drops across the electrode. Any readout errors from the reference electrode will impact the quantification of ion activity. In addition, experiments to explore the effect of membrane potential on specific transport mechanisms are not possible.

To overcome these limitations, we developed a novel approach to measure dynamic changes in the intracellular activity of transported ions in intact, isolated skeletal muscle fibers under current- or voltage-clamp control. For studies of electrogenic transport processes, this method allows simultaneous measurement of ion currents and any accompanying change in intracellular ion activities; for electroneutral transport processes, it provides measurement of the intracellular ion activity changes under conditions when the membrane potential is controlled. The ability to control the membrane potential with voltage- or current-clamp eliminates contributions from any interacting voltage-dependent membrane processes.

We impale a single fiber with four microelectrodes. Typically, one ISM and three standard intracellular microelectrodes are used, two to measure  $V_m$  and one to inject current (alternatively, two different ISMs can be used). The ISM is monitored using a dual-channel high-impedance amplifier compatible with high-resistance ISMs; membrane current and voltage are controlled by a second, high-voltage two-microelectrode voltage-clamp amplifier. The ability to fix the membrane potential allows the study of factors that both depend on and alter membrane potential, such as occurs with electrogenic ion transport mechanisms. In addition, the combined measurement of (net) membrane current ( $I_m$ ), and myoplasmic ion activity aids identification of the charge carrier.

We demonstrate this approach using examples that address specific questions about  $Cl^-$ ,  $H^+$ , and  $Na^+$  ion transport and homeostasis in skeletal muscle. The method can be easily extended to study other physiologically relevant ions in other cell preparations.

## Materials and methods

### Isolated muscle fibers

Studies were performed on short (<450- $\mu$ m) fibers enzymatically dissociated from FDB and interosseous muscles of C57BL mice, following previously described protocols (DiFranco et al., 2011; DiFranco and Vergara, 2011; Fu et al., 2011). In brief, mice were euthanized by deep anesthesia followed by cervical dislocation. An excised muscle was pinned to the bottom of a 3.5-cm Petri dish lined with Silgard and was enzymatically digested using 4 mg/ml type 2 collagenase (Worthington Biochemical Corporation) dissolved in HEPES-buffered Tyrode’s solution. Digestion was performed for 35 min using a shaking water bath at 35°C and 1 rpm. To release free fibers, the digested muscles were forced back and forth through progressively smaller-bore fire-polished Pasteur pipettes.

Single dissociated fibers were plated onto a 100- $\mu$ m-thick coverslip that formed the bottom of a 35-mm Petri dish. To increase adhesion, the dissociated free fibers were washed four to five times using HEPES-buffered Tyrode’s solution before plating (50–100 fibers). The fibers were kept in Tyrode’s solution at room temperature until use and were typically used within 1–8 h after dissociation.

The experimental chamber (~300  $\mu$ l) was continuously perfused at ~5 ml/min using a gravity-driven perfusion circuit. The solution level in the chamber was maintained constant by gentle suction. A steady solution level was found to be critical for maintaining a stable baseline current in voltage-clamp mode and for stability of potentials measured with the high-impedance amplifier for ion-sensitive microelectrodes. Solution exchanges were performed manually using multiport valves (Hamilton) in the perfusion circuit, and the chamber was completely exchanged within 1 s, as calibrated with a fluorescent dye. The standard recording solution was HEPES-buffered Tyrode’s solution, in mM: 140 NaCl, 4 KCl, 2 CaCl<sub>2</sub>, 1 MgCl<sub>2</sub>, 10 glucose, and 10 HEPES, pH 7.4 with NaOH, not gassed. For the pH studies in Fig. 4, a bicarbonate-buffered Tyrode’s solution was used, which consisted of, in mM: 118 NaCl, 4.75 KCl, 2.54 CaCl<sub>2</sub>, 1.18 MgSO<sub>4</sub>, 1.18 NaH<sub>2</sub>PO<sub>4</sub>, 24.8 NaHCO<sub>3</sub>, and 10 glucose, pH 7.4 when gassed with 95% O<sub>2</sub> and 5% CO<sub>2</sub>. The internal solution for the voltage-sensing microelectrodes ( $V_m$  and  $V_{ref}$ ), as well as the current-passing microelectrode ( $I_m$ ), comprised, in mM: 70 K-aspartate, 5 di-Na ATP, 5 di-Tris creatine phosphate, 40 EGTA, 20 morpholino propane sulfonic acid, and 5 MgCl<sub>2</sub>, pH 7.4 with KOH. The use of 40 mM EGTA reduces intracellular Ca<sup>2+</sup> to nanomolar concentrations and prevents contraction in current-clamp or voltage-clamp studies where large depolarizations are used. Alternatively, high EGTA is not needed when voltage changes are kept below the mechanical threshold. All procedures involving animals were approved by the University of California, Los Angeles Research Animal Committee.

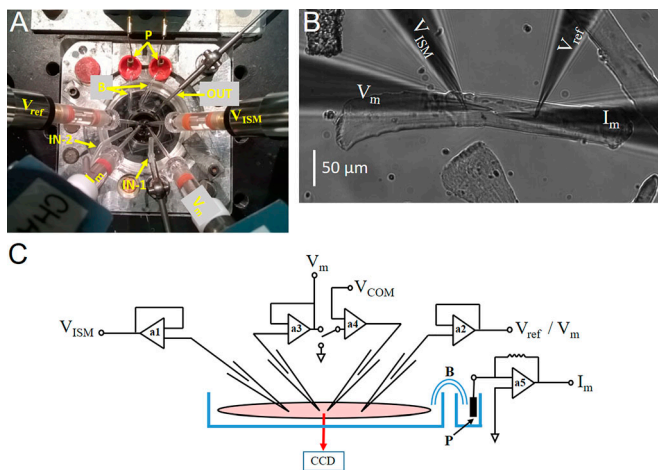


**Figure 1. A four-microelectrode method to measure intracellular ion activity in a voltage-clamped skeletal muscle fiber.** (A) Photograph of the recording chamber on the stage of an inverted microscope. An ISM ( $V_{ISM}$ ) and reference microelectrode ( $V_{ref}$ ) were connected to a high-input impedance amplifier to measure intracellular activity of  $\text{Na}^+$ ,  $\text{H}^+$ , or  $\text{Cl}^-$ . A second voltage-sensing microelectrode ( $V_m$ ) and current-passing microelectrode ( $I_m$ ) were used for the TEVC. The Ag/AgCl pellets (P) from the bath amplifier were connected to the recording chamber with salt bridges (B). IN-1 and IN-2 are independent solution inlets from two perfusion systems. OUT is the suction outlet. (B) Photomicrograph of a typical dissociated single fiber impaled with four microelectrodes. (C) Schematic diagram of the circuit used to measure  $V_{ISM}$ ,  $V_{ref}$ ,  $V_m$ , and  $I_m$ . A high-voltage TEV-200A amplifier (Dagan) was used to measure and control membrane potential and membrane current. An FD223a two-channel high-impedance ( $10^{15} \Omega$ ) amplifier (World Precision Instruments) was used to measure the voltage of two ISMs or the voltage of one ISM and one standard sharp intracellular reference microelectrode ( $V_{ref}$ ). a1 and a2, high-input preamplifiers for ISMs; a3, instrumentation amplifier for real-time calculation of  $V_{ion} = V_{ISM} - V_{ref}$ ; a4, membrane potential recording preamplifier of the voltage-clamp; a5, control amplifier connected to the current injection electrode; a6, bath control amplifier (for simplicity, only on salt bridge is shown). CCD, charge-coupled device;  $V_{COM}$ , command potential.

### The four-microelectrode system

The four-microelectrode setup (Fig. 1) was configured by combining a TEVC and a high-impedance electrometer with both a reference electrode and ISM inputs. With this system, the intracellular activity of one or two separate ions can be measured in dissociated muscle fibers maintained under either current- or voltage-clamp conditions.

A TEVC with a high compliance of 145 V (TEV-200A amplifier; Dagan) was used to optimize the clamp speed of fibers  $\leq 450 \mu\text{m}$  in length (membrane capacitance,  $C_m \sim 2 \text{ nF}$ ). Capacitance compensation was performed for both the voltage-sensing ( $V_m$ ) and current-passing ( $I_m$ ) microelectrodes of the TEVC before fiber impalement. The TEV-200A active bath clamp was used to maintain the bath at virtual ground in either current- or voltage-clamp modes. The sensing and current injection terminals of the bath amplifier were connected via salt bridges (with floating Pt wires) to the bath solution. A two-channel amplifier (FD223a; World Precision Instruments) with high-impedance inputs ( $>10^{15} \Omega$ , shunted by 0.5 pF) was used to measure the voltage of two ISMs or the voltage of one ISM and one standard sharp intracellular reference microelectrode ( $V_{ref}$ ). No capacitance compensation was possible for  $V_{ref}$  because the device

lacks this function. ISM electrodes cannot be compensated for capacitance. The ground terminals of both amplifiers were connected. For data to show fast transients in Fig. 2, the voltage signals ( $V_m$ ,  $V_{ref}$ , and the Na-dependent potential of the Na-ISM,  $V_{\text{Na-ISM}}$ ) were lowpass filtered at 10 kHz, the current ( $I_m$ ) was filtered at 5 kHz, and the data were sampled at 30  $\mu\text{s}$ . Records of several minutes were used for all other figures, and the sampling interval was 20 ms. When recording small-amplitude Na,K-ATPase currents (Fig. 5),  $I_m$  was filtered at 100 Hz to enhance the online detection of current amplitude.

The headstages of these amplifiers (preamplifiers a1, a2, a4, and a5 in Fig. 1) were attached to four micromanipulators (MPC285; Sutter Instruments) that were mounted on a custom stage of an inverted fluorescence microscope (IX-100; Olympus). The angle of approach was oriented with the TEVC microelectrode pair being collinear with the fiber axis and the two ISM microelectrodes both approaching from the same side of the fiber (Fig. 1). A standard video camera was attached to the trinocular port of the microscope and used for continuous observation on a monitor during microelectrode placement and impalement at various magnifications (10 $\times$ , 40 $\times$ , and 100 $\times$  oil). A charge-coupled device camera (Santa Barbara Instrument Group) attached to the lateral port of the microscope was used to obtain digital still images of whole impaled fibers (at 10 $\times$ ) for offline calculation of geometrical parameters (diameter, length, and surface area) using a custom algorithm.

### ISMs

Micropipettes for both sharp and ion-sensing electrodes were pulled from 1.5-mm borosilicate capillaries with internal microfilaments (BF150-86-10; Sutter Instruments). A four-step pulling protocol using a horizontal puller (P97; Sutter Instruments) was optimized to obtain a short shaft ( $\sim 8 \text{ mm}$ ) leading to a submicrometer tip opening. The electrodes had a tip resistance of 10–12 M $\Omega$  when filled with internal solution (typically 100 mM monovalent salts). The use of capillaries with microfilaments significantly speeded the manufacture of ISMs without compromising the sealing of the organic phase to the inner face of the capillary wall. Capillaries were used as sold, without additional cleaning.

Silanized micropipettes must be used for ISM fabrication because the hydrophobic surface is essential for mechanical stability and high electrical resistance at the interface between glass and the liquid membrane at the tip of the electrode. Micropipettes were silanized by evaporation of chlorotrimethylsilane (Sigma-Aldrich) in a 500-ml jar, followed by baking at 250 $^\circ\text{C}$  for  $\geq 4 \text{ h}$ , as previously described (DiFranco et al., 2019). Silanized micropipettes were stored dry in a closed jar (Jar-E215; World Precision Instruments) to avoid dust adhesion and were used for  $\leq 2 \text{ wk}$  without noticeable deterioration.

ISMs were assembled by backfilling through a 34-G micro-needle, as previously described (DiFranco et al., 2019). Briefly, an excess of the ionophore-containing cocktail was delivered as closely as possible to the micropipette tip. Within a few minutes, the mixture spontaneously wicks into the tip and the excess is removed with a new clean microneedle until a layer only

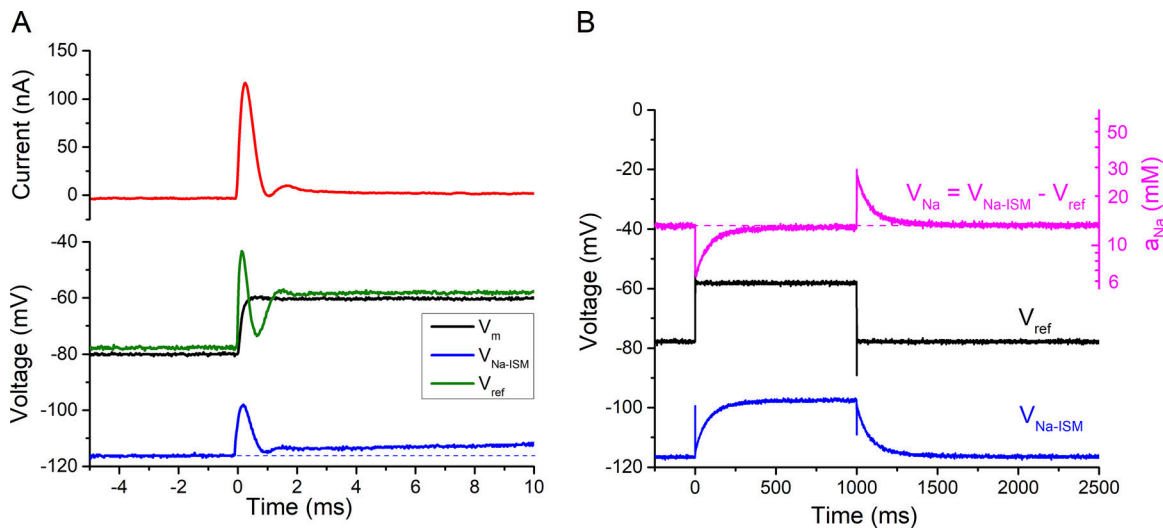


**Figure 2. Settling time for  $V_{Na-ISM}$  under voltage clamp. (A)** The voltage-clamp response for a 20-mV depolarization from  $-80$  mV is shown on a fast time scale. The current transient (top panel, red) settled within 1 ms and had only a small oscillation (1–1.5 ms). Simultaneous recordings from the three voltage-sensing microelectrodes (bottom panel) show that the rapid step change in  $V_m$  was completed in  $<1$  ms ( $V_m$ , black). The voltage signals from the high-impedance amplifier ( $V_{ref}$ , green;  $V_{Na-ISM}$ , blue) had larger oscillations for the first 2 ms because this device has no analogue capacitance compensation. The response time of the  $V_{Na-ISM}$  is slow, as shown by the depolarizing shift relative to the dashed line, and does not reach steady state during this 10-ms trace. **(B)** A long-duration depolarization of 20 mV shows the settling time of the  $V_{Na-ISM}$ , which in this example had a time constant of 80 ms. The intracellular  $Na^+$  activity ( $a_{Na}$ ) did not change in response to the depolarization, as shown by the stable  $V_{Na} = V_{Na-ISM} - V_{ref}$  corresponding to an activity of 13.2 mM (dashed line, magenta).

200–300  $\mu\text{m}$  remains. The saline solution is then backfilled with another microneedle, taking care to ensure a clean interface with the organic layer and no bubbles. Before use, each ISM was individually tested using the calibration solutions. Acceptable electrodes were stored in sealed jars (Jar-E215; World Precision Instruments) with tips submersed in filtered (0.2  $\mu\text{m}$ ) saline. ISMs were used up to 2 wk after fabrication, with no detectable deterioration.

The ionophore cocktails were mixed and stored as stock solutions at room temperature that could be used for up to 1 yr. The composition (wt/wt %) of the ionophore and the backfilling saline solutions were, for the sodium microelectrode (Na-ISM), 10%  $Na^+$  ionophore IV (#71745; Sigma-Aldrich), 1% Na-tetraphenylborate in 2-nitrophenyl octyl ether (NPOE), backfilled with 100 NaCl and 10 HEPES, pH 7.4 titrated with HCl; for the chloride microelectrode (Cl-ISM), 10% mercuracarborand-3 (custom synthesized; DiFranco et al., 2019), 2.5% tridodecylmethyl ammonium chloride in NPOE, backfilled with 100 NaCl and 10 HEPES, pH 7.4 titrated with  $H_2SO_4$ ; and for proton (pH) microelectrode (H-ISM), 10%  $H^+$  ionophore-I (#95292; Sigma-Aldrich), 0.7% tetraphenylborate in NPOE, backfilled with 100 NaCl and 100 HEPES, pH 7.0 with HCl.

### Calibration of ISMs

A three-point calibration check was used immediately after ISM fabrication to select high-quality electrodes. We verified that all three types of ISMs had linear Nernstian responses over the physiological ranges of interest (1–100 mM for  $Na^+$  and  $Cl^-$ , 6.0–8.0 pH units for H), wherein  $V_{ion-ISM}$  was proportional to the logarithm of ion activity,  $\log(a_{ion})$ .

The calibration solutions, prepared as molar concentration, were converted to activity for the ion of interest,  $a_{ion}$ , by using the extended Debye–Hückel equation (Davies, 1962), which accounts for both ionic strength and ionic radius. For the Na-ISM, calibration solutions of 1, 10, and 100 mM  $Na^+$  were prepared by mixing 150  $Na^+$  stock solution (in mM: 150 NaCl, 7.2 TEA-OH, and 10 HEPES, pH 7.4 with TEA-OH) and 160 NMDG stock solution (in mM: 160 NMDG and 10 HEPES, pH 7.4 titrated with HCl). For the Cl-ISM, calibration solutions of 1, 10, and 100 mM  $Cl^-$  were prepared by mixing 150  $Cl^-$  stock solution (in mM: 140 NaCl, 4 KCl, 2  $CaCl_2$ , 1  $MgCl_2$ , and 10 HEPES, pH 7.4 with NaOH) and 0  $Cl^-$  stock solution (in mM: 115  $Na_2SO_4$ , 2  $K_2SO_4$ , 2  $Ca(OH)_2$ , 1  $Mg(OH)_2$ , and 10 HEPES, pH 7.4 titrated with  $H_2SO_4$ ). For the H-ISM, calibration solutions of varying pH were prepared from Tyrode's stock solution for which the buffer at 10 mM was either 2-(*N*-morpholino)ethanesulfonic acid (pH 6.0 or 6.5), HEPES (pH 7.0 or 7.5), or Tris (pH 8.0).

The offset of each ISM was set to 0 mV in the following solutions to facilitate the online interpretation of ionic activity during an experiment: 100 mM Na-Tyrode's solution for Na-ISM, 100 Cl-Tyrode's solution for Cl-ISM, and HEPES buffered (pH 7.0) Tyrode's solution for H-ISM.

For intracellular measurements, the voltage of the ISM was  $V_{ion-ISM} = V_{ion} + V_m$ , where  $V_{ion}$  is the electrochemical potential detected by the selective ionophore, and  $V_m$  is the membrane potential of the cell. The value of  $V_m$  used for calculating  $a_{ion}$  was measured as the potential detected by the reference microelectrode ( $V_{ref}$ ) of the high-impedance amplifier. Digital subtraction was used to compute  $V_{ion} = V_{ion-ISM} - V_{ref}$ . Finally, ion activity was calculated as  $a_{ion} = a_0 \times 10^{(V_{ion}/k)}$ , where  $a_0$  is the activity of the control solution when  $V_{ion}$  is set to 0 mV, and  $k$  is the slope of

the linear relation between  $V_{ion}$  and  $\log(a_{ion})$ . At the end of the experiment, the ISM was withdrawn from the fiber, and the stability of the three-point calibration was verified with the same solutions used for the initial screen of ISM quality.

## Results

### Fiber impalement and quality of the voltage clamp

We have previously demonstrated that high-quality voltage clamp recordings can be achieved in intact, short (<450- $\mu\text{m}$ ) mammalian skeletal muscle fibers by using a high-voltage two-microelectrode voltage clamp (DiFranco et al., 2011; DiFranco and Vergara, 2011; Fu et al., 2011). This approach can be used to obtain reliable measurements of the major ionic currents (DiFranco et al., 2011, 2012, 2015b; DiFranco and Vergara, 2011; Fu et al., 2011) and transport mechanisms (DiFranco et al., 2015a) in skeletal fibers.

A top view of the four-electrode configuration is shown in Fig. 1 A, demonstrating the placement of microelectrodes, salt bridges, and perfusion components around the experimental chamber mounted on the stage of the inverted microscope. Ideally, the four microelectrodes would be oriented orthogonally from each other to reduce capacitance coupling between electrodes. The actual orientation that we achieved is smaller ( $\sim 60^\circ$ ) due to space constraints from the two salt bridges and virtual-ground preamplifier. The salt bridges connect the bath solution to the voltage measuring and current output of the virtual ground amplifier and are essential to limit changes in junction potentials upon bath solution changes.

The  $V_m$  and  $I_m$  microelectrodes of the two-electrode voltage-clamp (TEVC) were located near the center of the fiber with a separation of  $\sim 20 \mu\text{m}$ , and the ion-sensing microelectrode pair,  $V_{ISM}$  and  $V_{ref}$ , were placed more laterally  $\sim 100 \mu\text{m}$  from each end of the fiber (Fig. 1 B). Clean electrode impalements with minimal damage to the fiber were achieved with the following protocol. First, the TEVC microelectrodes were inserted into the fiber. Small current pulses (4–5 nA, 5 ms) were applied at 3 Hz through the  $I_m$  electrode in current-clamp mode while it was slowly advanced toward the fiber. Contact with the membrane was signaled by an increase in the voltage drop at the electrode tip (i.e., an increase in tip resistance). A small additional advance of the microelectrode led to membrane puncture, as evident from a sudden change in steady potential (–45 to –65 mV) and a reduction of the voltage drop during the pulse. Fiber impalement with the  $V_m$  microelectrode was performed next, and again an abrupt change in voltage plus the membrane charging in response to the injected current pulse were used to detect membrane penetration rather than a change in visual appearance. A small holding current (<10 nA in high-quality fibers of length up to 450  $\mu\text{m}$ ) was then applied in current-clamp mode to bring the resting potential to –80 mV. As the fiber recovered over the next 3–5 min, the holding current required to maintain a  $V_m$  of –80 mV usually decreased.

Next, the ion-sensing microelectrodes were inserted into the fiber. Impalement with the  $V_{ref}$  microelectrode was detected by an abrupt voltage change from 0 mV to within 2 or 3 mV of the holding potential of –80 mV, as reported by the  $V_m$  electrode.

Confirmation was obtained by measuring the  $V_{ref}$  voltage transient in response to a 5-nA current pulse applied through the  $I_m$  microelectrode. Finally, an ISM (for  $\text{Na}^+$ ,  $\text{Cl}^-$ , or  $\text{H}^+$ ) was inserted into the fiber. Impalement was detected as a voltage jump, recognizing that the amplitude is the sum of  $V_{ion} + V_m$ , +65 – 80 = –15 mV for  $\text{Cl}^-$  and –40 – 80 = –120 mV for  $\text{Na}^+$ .

Several criteria were used to define a successful four-electrode preparation. First, the initial holding current should be small (<20 nA) to maintain a holding potential of –80 mV. Second, the holding current should not increase >50% with the subsequent insertion of the ISM microelectrodes. Third,  $V_m$  and  $V_{ref}$  should agree within 3 mV. Fourth,  $V_{ISM}$  should be near the expected value of  $V_{ion} + V_{ref}$ . Finally upon withdrawal from the fiber at the end of the experiment, the voltage-sensing microelectrodes ( $V_m$  and  $V_{ref}$ ) in the standard HEPES-buffered Tyrode's solution should read  $0 \pm 3$  mV, and a repeat of the three-point calibration of the  $V_{ISM}$  should be within 3 mV of the values obtained before impalement. In a random sample of 24 preparations for which all four microelectrodes were successfully inserted, 21 from the sample met all these criteria.

### Response time of an ISM in a voltage-clamped fiber

One goal of the present work was to demonstrate that an electrically stable condition can be achieved when short flexor digitorum brevis (FDB) fibers, already impaled with two sharp microelectrodes connected to the voltage-clamp amplifier, are also impaled with one or two additional ISMs connected to another (high-impedance) amplifier. Conversely, we verified that the ISM performance is not adversely affected by the voltage-clamp amplifier working in either current- or voltage-clamp configuration.

The response of an FDB fiber impaled with four microelectrodes ( $V_m$  and  $I_m$  for TEVC, plus  $V_{ref}$  and  $V_{Na-ISM}$ ) is shown in Fig. 2. The fiber was held at –80 mV in voltage-clamp mode. The holding current was small (–3.5 nA) and did not drift, which shows that the fiber was healthy and without signs of damage from microelectrode impalement. As expected, the  $V_{Na-ISM}$  signal (blue trace) was more negative than  $V_m$  because the ISM was initially zeroed in a 100-mM  $\text{Na}^+$  solution, whereas intracellular  $\text{Na}^+$  activity ( $a_{Na}$ ) is  $\sim 10$  mM. The quality of the voltage clamp is shown by the response to a 20-mV step depolarization on a fast time scale (Fig. 2 A). The clamp speed was comparable to the performance we see in fibers studied with a conventional TEVC alone (DiFranco et al., 2011; Fu et al., 2011). With a clamp feedback gain of  $\sim 75\%$ , both the capacitance transient of  $I_m$  (red trace) was complete and  $V_m$  (black trace) reached steady state in <1 ms, and the measured membrane potential change ( $V_m$ , 10-kHz bandwidth) closely followed the imposed 20-mV step. The voltage clamp was stable, without large oscillations detected in  $V_m$  or  $I_m$ . The potentials measured with the FD223a amplifier had transient biphasic oscillations ( $V_{Na-ISM}$ , blue trace;  $V_{ref}$ , green trace) at the onset of the pulse, most likely because these electrodes cannot be compensated for capacitance. Importantly, the voltage detected by  $V_{ref}$ , placed  $\sim 100 \mu\text{m}$  from  $I_m$ , was comparable to  $V_m$  sensed by the voltage clamp and attests to the quality of the space clamp. Therefore, we are confident that the local membrane potential at the site of the ion-sensing microelectrode

is also equal to  $V_m$ . This constance is essential, because  $V_{ion}$  is derived from  $V_{ion-ISM} - V_{ref}$ , and the corresponding interpretation of ion activity is exponentially related to this difference. In practice,  $V_{ref}$  was always within a few millivolts of  $V_m$ , which implies that the  $V_{ref}$  microelectrode can be omitted to reduce the complexity of the system (and potential damage to the fiber). Alternatively, a second  $V_{ion-ISM}$  can be used so that two different intracellular ion activities can be measured simultaneously or the second  $V_{ion-ISM}$  can be placed just outside the fiber to obtain a direct measure of the local transmembrane ion gradient. A slowly depolarizing drift was observed for  $V_{Na-ISM}$  after the pulse onset (Fig. 2 A, blue trace) because, on the short time scale of 10 ms, the response had not reached the steady-state value of  $-100.3$  mV at 1,000 ms.

The response to a long-duration voltage step is shown for a different FDB fiber in Fig. 2 B. The response of the Na-ISM (blue trace) exponentially approached steady state with a time constant of  $\sim 80$  ms. This lag in the  $V_{Na-ISM}$  response is typical for a high-impedance ISM, as contrasted with the fast response of the reference microelectrode  $V_{ref}$  (black trace) to measure membrane potential. Because the settling times of these two microelectrodes are different, the subtraction used to compute the electrochemical potential for  $Na^+$  across the liquid membrane of the ISM,  $V_{na} = V_{Na-ISM} - V_{ref}$  will transiently be invalid after each voltage jump. This effect is shown by the  $V_{Na}$  signal (magenta trace) in Fig. 2 B. At the onset of the 20-mV depolarization ( $t = 0$  ms), the difference signal,  $V_{Na}$ , had an apparent decrease that returned to baseline within 500 ms (i.e., four time constants of  $V_{Na-ISM}$ ), as would be expected for a constant intracellular  $Na^+$  activity. The mirror-image effect occurs at the off edge of the pulse. While this temporal bandwidth limitation of ISMs is well known (Ammann, 1986), our four-microelectrode setup provides a new method to directly measure the ISM settling time while the electrode is in the intracellular environment. Alternatively, the voltage clamp can be used to hold  $V_m$  constant, even in the face of bath solution exchanges, drug application, or other perturbations, which ensures that a change in the  $V_{ion-ISM}$  signal is caused by a change of intracellular ion activity,  $a_{ion}$ , and not a shift of the membrane potential.

### Voltage-dependent changes of intracellular $Cl^-$ activity

The membrane properties of skeletal muscle enabled us to test the ability of our four-microelectrode setup to detect a voltage-dependent shift of intracellular ion activity. The chloride conductance is especially large in resting muscle,  $\sim 1$  mS/cm<sup>2</sup> (Dulhunty, 1979; Pedersen et al., 2009), whereas the active transport of  $Cl^-$  by cotransporters and exchangers is small in comparison ( $\sim 15$  pmol/cm<sup>2</sup>; Geukes Foppen, 2004). Because of this arrangement, the equilibrium potential for  $Cl^-$  ( $E_{Cl}$ ) is only a few millivolts depolarized from the membrane potential (Aickin et al., 1989). If a sustained change of  $V_m$  is imposed, then the prediction is that intracellular  $Cl^-$  will shift until  $E_{Cl}$  is again only a few millivolts depolarized relative to  $V_m$ . While indirect evidence in support of this concept has been provided (Aickin et al., 1989), there has never been a direct measurement showing a change of intracellular  $a_{Cl}$  in response to an imposed shift of  $V_m$ .

The intracellular  $Cl^-$  activity,  $a_{Cl}$ , measured from FDB fibers with our four-microelectrode setup in either voltage-clamp mode or current-clamp mode, is shown in Fig. 3. As before, the  $V_m$  response of the clamp and the  $V_{ref}$  signal were nearly identical (black and blue traces, respectively, in top panel of Fig. 3 A). The voltage sensed by the  $Cl^-$ -ISM was close to 0 mV (red trace), because  $E_{Cl}$  was only a few millivolts depolarized from  $V_m$ . On the time scale of hundreds of seconds in this figure, the slow transients in the  $V_{Cl-ISM}$  trace were caused by shifts of intracellular  $a_{Cl}$  (not the settling time of the ISM, which is  $< 1$  s, Fig. 2). Also note that for this anion-selective ISM, the voltage becomes more negative as the intracellular  $a_{Cl}$  increases. The change of intracellular  $a_{Cl}$  is shown more clearly by computing  $V_{Cl} = -(V_{Cl-ISM} - V_{ref})$ , as shown in the bottom panel of Fig. 3 A (green trace). The inset shows an excerpt of the total membrane current,  $I_m$  (gray), which is primarily a  $Cl^-$  current, because other conductances inactivate on this slow time scale or are much smaller. In support of this interpretation, the amounts of charge conducted in response to these three voltage jumps were 0.29, 0.63, and 0.98  $\mu C$  (area under each transient), which for the accessible fiber volume of  $0.62 \times 10^{-6}$  cm<sup>3</sup> corresponds to a calculated  $\Delta a_{Cl}$  of 3.3, 7.2, and  $-11.3$  mM and is comparable to the measured changes of intracellular  $a_{Cl}$  (green trace) of 3.6, 7.2, and  $-10.8$  mM. Finally, at the end of the record (700–1,100 s), the  $Cl^-$ -ISM was withdrawn from the fiber, and the electrode calibration was repeated.

The response of a different FDB fiber under current clamp is shown in Fig. 3 B. Again, the  $V_{Cl}$  potential is negative and close to 0 mV because intracellular  $a_{Cl}$  shifts until  $E_{Cl}$  is a few millivolts more positive than  $V_m$ . A step change in applied current produced an initial rapid depolarization, from the usual passive resistor-capacitor properties of the membrane, that was followed by a slow depolarization of  $V_m$  as intracellular  $Cl^-$  accumulated. The  $V_{Cl-ISM}$  response was almost flat because  $E_{Cl}$  and  $V_m$  shifted in parallel. The change of intracellular  $a_{Cl}$  was substantial, however, as shown by the difference trace  $V_{Cl} = -(V_{Cl-ISM} - V_m)$ . Also notice that  $V_{Cl}$  did not have an initial rapid transition like  $V_m$ , because intracellular ion activity only changes slowly.

These data clearly show that substantial shifts of intracellular  $a_{Cl}$  occur in intact muscle fibers when a sustained shift of  $V_m$  is imposed. Moreover, these data provide the first measure for the time course of the  $a_{Cl}$  shift, which had a time constant on the order of 3–10 s.

### Absence of voltage-dependent changes of intracellular pH demonstrated with a proton-selective microelectrode

We used a pH-sensitive ISM with the four-microelectrode setup to demonstrate a shift of intracellular  $H^+$  activity,  $a_H$ , produced by exchange of the bath solution and also to show that the difference signal,  $V_H = V_{H-ISM} - V_{ref}$ , was insensitive to an imposed voltage jump of  $V_m$ . The fiber was initially held at  $-80$  mV in voltage-clamp mode, as shown in Fig. 4. Again, the  $V_m$  and  $V_{ref}$  signals were indistinguishable (black and blue traces, respectively), and the  $V_{H-ISM}$  potential (red trace) was more negative than  $V_{hold}$  because this ISM was zeroed in a pH-7.0 calibration solution. The difference signal,  $V_H = V_{H-ISM} - V_{ref}$  (green trace), is proportional to intracellular pH, as shown by the ordinate

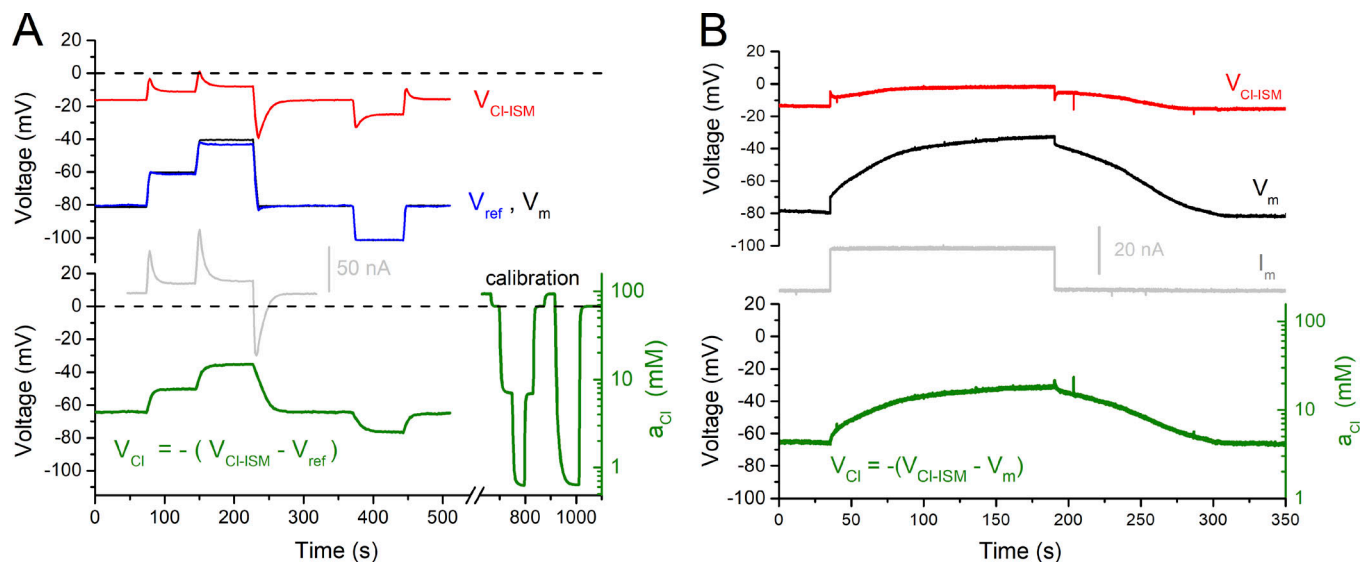


**Figure 3. Voltage-dependent movement of chloride ions. (A)** Upper panel: Simultaneous recordings of  $V_m$  (black),  $V_{ref}$  (blue), and  $V_{Cl-ISM}$  (red) from a fiber under voltage clamp. The Cl-ISM was initially zeroed in modified Tyrode's solution with a  $[Cl^-]$  of 100 mM, corresponding to  $a_{Cl} = 69$  mM. The Cl potential,  $V_{Cl} = -(V_{Cl-ISM} - V_{ref})$ , was computed offline and is plotted in the lower panel, along with the calibration response for the Cl-ISM that was performed after the electrode was withdrawn from the fiber. The inset in the lower panel shows a portion of the  $I_m$  trace (gray) to illustrate the membrane current transients associated with the changes of intracellular  $Cl^-$ . Fiber depolarization induced a substantial increase of intracellular  $a_{Cl}$ , with a time constant of  $\sim 5$  s and was fully reversible, albeit slower (time constant  $\sim 10$  s), with repolarization of the fiber. The chamber was continuously perfused with HEPES-buffered Tyrode's solution. **(B)** The response of a different FDB fiber is shown under current clamp. The step change in applied current caused an abrupt change in membrane potential (the resistor-capacitor, "RC," of the membrane;  $V_m$ , black trace), followed by a slow transient caused by the accumulation of intracellular  $Cl^-$ . The  $V_{Cl}$  trace (green, lower panel) had a smooth slow transient, as expected for the accumulation and then depletion of intracellular  $Cl^-$ .

scale on the right in Fig. 4. The control bath solution was HEPES-buffered Tyrode's solution (pH 7.4) that contained no bicarbonate and was not gassed with  $CO_2$ , which results in intracellular alkalosis, as shown by the initial pH of  $\sim 7.85$  (interval 0–2 min). Bath exchange with a 24-mM  $HCO_3^-$ -buffered Tyrode's solution that was preequilibrated with 5%  $CO_2/95\%$   $O_2$  (pH 7.4) caused a rapid decrease of intracellular pH to 7.45 (Fig. 4, interval 2–7 min) that was reversible upon return to  $HCO_3^-/CO_2$ -free Tyrode's solution.

A second bath exchange back to 5%  $CO_2$  was performed at 12 min, followed by a 30-mV step depolarization (Fig. 4, 17–20 min). The  $V_{H-ISM}$  signal had a nearly identical step change in voltage (red trace, 17–20 min) on this time scale of minutes for which the settling time for the ISM was much faster. Consequently, the difference signal that yields  $V_H$  had no significant change (green trace), as expected when the intracellular pH remains constant.

#### Demonstration of electrically silent and electrogenic $Na^+$ transport in a voltage-clamped fiber

The combined ability to measure ion activity with an ISM and to voltage-clamp the cell is a powerful approach that can be used to study a variety of transport mechanisms. We show an example where the four-microelectrode setup was used to measure intracellular  $Na^+$  accumulation/depletion in response to modulation of Na,K-ATPase pump activity imposed by changing external  $[K^+]$ . Our prior voltage-clamp studies showed that in isolated fibers, the current generated by electrogenic pump transport,  $I_{pump}$ , can be stimulated by increasing external  $[K^+]$

from 4 to 20 mM (20K condition) or stalled by removing  $K^+$  from the external solution (OK condition), and that this process is reversible (DiFranco et al., 2015a). It is predicted that these changes in pump activity will cause commensurate changes in intracellular  $Na^+$ , which in turn will modulate pump activity; however, this has not been directly measured in skeletal muscle.

Fig. 5 shows, for the first time, simultaneous measurements of intracellular  $a_{Na}$  and  $I_{pump}$  in a fiber voltage-clamped at  $-85$  mV while pump activity was modulated by step changes of external  $[K^+]$  from 0 to 20 mM. When the pump was stalled in the OK condition, intracellular  $Na^+$  rapidly increased, as shown by the depolarized shift of  $V_{Na-ISM}$  (Fig. 5 A, red trace). The Na-ISM potential was converted to  $a_{Na}$  and plotted in Fig. 5 C to illustrate the substantial magnitude of this intracellular  $Na^+$  accumulation. This  $Na^+$  load was then rapidly cleared when the Na,K-ATPase was reactivated by a return to the 20K condition. The process was fully reversible and could be repeated over several cycles, which demonstrates the stability of the preparation even with a fiber impaled by four microelectrodes.

As we previously reported from studies with a traditional TEVC (DiFranco et al., 2015a), a large transient pump current was rapidly activated by the transition from OK to 20K (Fig. 5 B). This net outward current reflects the 3  $Na^+ : 2 K^+$  stoichiometry of the Na,K-ATPase. The decay of  $I_{pump}$  correlates with the reduction of intracellular  $a_{Na}$ , demonstrating the well-known regulatory effect of  $Na_i$  on pump activity. In contrast to the clear electrogenicity of  $Na^+$  clearance by the Na,K-ATPase,  $Na^+$  loading while the pump was stalled in OK was almost silent electrically: Only a brief inward current surge was observed at the

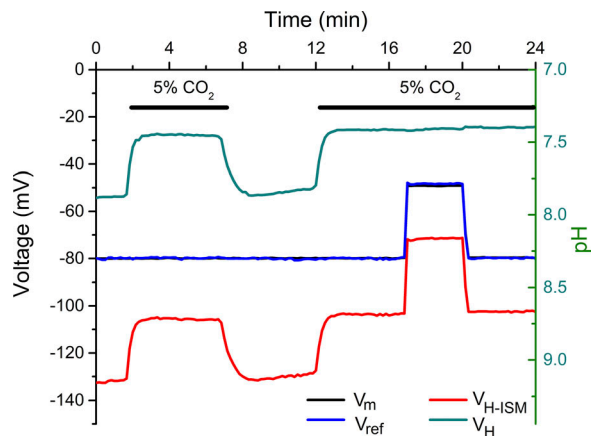


**Figure 4. Intracellular pH rapidly responds to CO<sub>2</sub> but is insensitive to a step depolarization of V<sub>m</sub>.** Traces show simultaneous recordings of V<sub>m</sub> (black), V<sub>ref</sub> (blue), and V<sub>H-ISM</sub> (red) from a fiber perfused with HEPES-buffered Tyrode's solution (pH 7.4, nominally 0 CO<sub>2</sub>) that was intermittently exchanged with Tyrode's solution containing 24 mM HCO<sub>3</sub><sup>-</sup> and gassed with 5% CO<sub>2</sub>, pH 7.4. The fiber was voltage-clamped at -80 mV, and before impalement, V<sub>H-ISM</sub> was zeroed in the presence of Tyrode's solution adjusted to pH 7.0. The proton potential, V<sub>H</sub> = V<sub>H-ISM</sub> - V<sub>m</sub> (green), was computed digitally offline and is proportional to pH (right ordinate). Intracellular pH was alkaline (~7.9) in CO<sub>2</sub>/HCO<sub>3</sub><sup>-</sup>-free Tyrode's solution and rapidly acidified to 7.4 in the presence of CO<sub>2</sub>. A 30-mV step depolarization of V<sub>m</sub> produced an identical shift of V<sub>H-ISM</sub>; therefore, the difference between these two potentials remained constant (green trace, 16–20 min), indicating no change of V<sub>H</sub> with a constant pH.

onset of the OK condition. Presumably most of the net Na<sup>+</sup> entry occurs via an electroneutral exchanger or cotransporter (but not the NKCC1 cotransporter, which would be inactive in OK, or Na/HCO<sub>3</sub> exchangers in this bicarbonate-free preparation).

These data also provide a new method to characterize the dependence of pump activity on intracellular a<sub>Na</sub>. The data from Fig. 5 (B and C) are redrawn as a phase-plot of I<sub>pump</sub> versus a<sub>Na</sub> in Fig. 5 D. Starting from the lower left corner of the plot (low a<sub>Na</sub> in 2OK), the transition to OK causes Na<sup>+</sup> loading with very little change in I<sub>m</sub> (horizontal trajectory to the right). From here, the transition back to 2OK produces an abrupt increase in I<sub>pump</sub> (steep upward segment). The high Na,K-ATPase activity then causes intracellular a<sub>Na</sub> to decrease (leftward movement), which in turn decreases I<sub>pump</sub> (downward movement) until the trajectory returns to the starting point. This upper limb of the closed-loop, labeled Na<sup>+</sup> clearance in the plot provides a direct measure of Na,K-ATPase activity as a function of intracellular a<sub>Na</sub> for a given constant external [K<sup>+</sup>].

## Discussion

### Combined voltage-clamp and ISM recording is robust in muscle fibers

Our experience with a new four-microelectrode technique firmly establishes the feasibility of simultaneously using an ISM to measure intracellular ion activity while also performing voltage-clamp recordings from dissociated muscle fibers. The addition of the V<sub>ISM</sub> and V<sub>ref</sub> electrodes did not compromise the clamp speed or cause the clamp to become unstable and oscillate

(Fig. 2). Furthermore, the close agreement of V<sub>ref</sub> (ion-sensing circuit) and V<sub>m</sub> (TEVC circuit) confirmed the high quality of the space-clamp in these short fibers. Viewed from the alternate perspective, we showed that the quality of the ISM recording was not adversely impacted by the voltage clamp. The extraordinarily high impedance of the ISM circuit makes the system susceptible to noise from electromagnetic activity in the environment. In our experience, however, the output of the ISM circuit, V<sub>ion</sub> = V<sub>ion-ISM</sub> - V<sub>ref</sub>, remained stable and free from artifact while the fiber was voltage-clamped, and even when a step change of V<sub>m</sub> was imposed (Fig. 4).

The fiber impalement with four microelectrodes was well tolerated, and the muscle preparation remained viable, with stable responses often lasting an hour or longer. Several criteria support our interpretation that fibers remained healthy in the four-microelectrode configuration. First, the resting potential remained relatively constant (±3 mV), even as the second and third microelectrodes were inserted (V<sub>rest</sub> cannot be measured in isolation for the fourth, ISM, electrode). Second, in voltage-clamp mode, only a small current (approximately -5 nA) was required to hold V<sub>m</sub> at -80 mV, and this current did not drift over time. The preparation was stable enough to reliably measure small Na,K-ATPase pump currents of 5–10 μA/cm<sup>2</sup> over a 30-min interval (Fig. 5). Third, the measured activity of intracellular Na<sup>+</sup>, H<sup>+</sup>, and Cl<sup>-</sup> remained constant over tens of minutes, under conditions where V<sub>m</sub>, pump activity, and bath composition were held constant, implying that there were no substantial leakage currents that would dissipate ion gradients.

Prior studies with self-referencing ISMs constructed from double-barreled theta glass capillaries often showed signs of fiber damage with low resting potentials and unstable recordings with drift (Aickin and Brading, 1982; Kondo et al., 1993). Our design with separate V<sub>ref</sub> and V<sub>ISM</sub> electrodes allows for smaller tip sizes than typically used with theta glass, which may account for the improved fiber viability. Our multiple (single-barrel) electrode technique for measuring intracellular ion activity while also in voltage-clamp could be adapted for use in other preparations with large cells such as *Xenopus* oocytes (Virkki et al., 2002) or invertebrate neurons.

### Technical advances from using the four-microelectrode system

The ability to measure intracellular ion activity with ISMs in a voltage-clamped fiber is an important advance for the study of ion gradients in skeletal muscle and provides new opportunities to investigate ion transport systems. Of the available methods to measure intracellular ion content, the ISM technique has several advantages: (a) a large linear operating range, approximately four orders of magnitude; (b) direct measurement of the most relevant property, ion activity; (c) measurement of absolute activity, not relative; (d) stability over tens of minutes, with very little drift; (e) availability of highly selective ionophores for most ions of interest; and (f) low cost and equipment requirements. Another advantage is that the ISM method provides a simultaneous measure of V<sub>m</sub>, and now in the four-electrode configuration, I<sub>m</sub> is measured as well. Optical methods based on fluorescent dyes or genetically encoded indicators have also



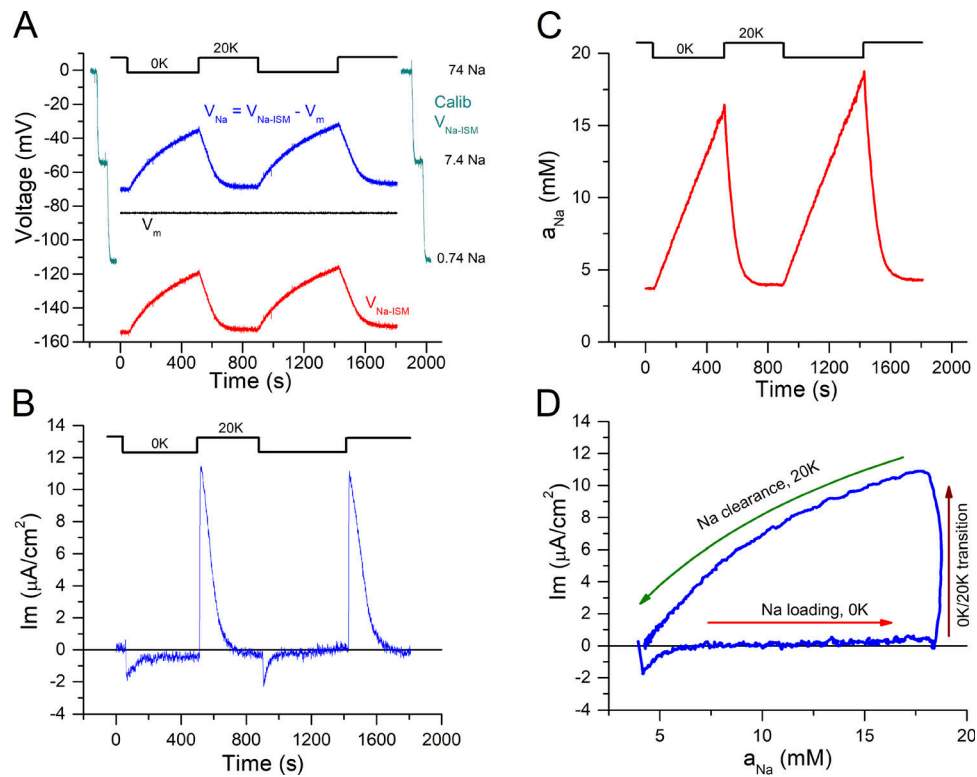


**Figure 5. Passive and active sodium translocation at a constant membrane potential.** (A) Simultaneous records of  $V_m$  (black trace) and  $V_{Na-ISM}$  (red trace) from a voltage-clamped fiber maintained at a holding potential of  $-85$  mV. Extracellular  $[K^+]$  was switched between 0 and 20 mM (compensated by replacement with  $Na^+$ ) in a continuously perfused chamber. The Na-dependent potential (blue trace) was computed as  $V_{Na} = V_{Na-ISM} - V_m$ . Inhibition of the Na,K-ATPase in 0 mM  $K^+$  caused a rise of  $[Na]$ , that was reversed in 20 mM  $K^+$ .  $V_{ref}$  was indistinguishable from  $V_m$  and is omitted. The traces shown at each side of the intracellular records represent the precalibration (left) and postcalibration (right) traces of the Na-ISM. (B) Membrane current density recorded simultaneously with the voltage records in A. Electrogenic extrusion of intracellular  $Na^+$  by the Na,K-ATPase produced a large outward current transient.  $I_m$  was zeroed in the presence of 20 mM  $K^+$ .  $K^+$ ,  $Ca^{2+}$ , and  $Cl^-$  currents were blocked using  $Ba^{2+}$  (1 mM), nifedipine (20  $\mu$ M), and 9-anthracene carboxylic acid (200  $\mu$ M), respectively. (C) Intracellular  $Na^+$  activity was calculated from  $V_{Na} = V_{Na-ISM} - V_m$ . (D) Phase plot of membrane current density as a function of the intracellular  $Na^+$  activity. Data are the responses in the time interval 800–1,800 s in B and C.

been used to measure intracellular ion concentration (unbound fraction) under voltage-clamp or current-clamp conditions (Tsien, 1989; Chen et al., 2013). These approaches may also provide complementary information such as spatial localization, targeting of the indicator to a subcellular compartment, faster kinetics, or labeling of a specific subset of cells in a heterogeneous background such as the central nervous system. However, their calibration requires accurate monitoring of dye concentration, which is not possible for many ion indicator dyes. While the concentration of  $Ca^{2+}$  indicator dyes can be calibrated dynamically using a ratiometric method, this is not possible with many other currently available dyes, e.g., Na- and K-indicators. The intracellular concentration of membrane-permeant (e.g., acetoxymethyl) dyes is not constant but can change during the measurement period as the indicator accumulates in the cell or within organelles; however, only a single calibration point is possible at the end of the measurement. Finally, the dynamic range for measuring ion concentrations is smaller with indicator dyes than for ion-sensitive microelectrodes.

With the ISM technique, fiber impalement with microelectrodes may cause a run-down of  $V_{rest}$ . If the ion gradient is sensitive to  $V_m$ , as we show here for  $Cl^-$  (Fig. 3), then the depolarization from impalement may cause an unwanted change

of intracellular ion activity. The addition of the voltage clamp avoids this concern and adds new capabilities to the recording system. First, the voltage clamp can be used to maintain  $V_m$  at the value of  $V_{rest}$  determined from the initial impalement of the fiber. The ability to maintain a constant  $V_m$  is also advantageous when studying the effects of perturbations (e.g., drugs or changes in external ion concentration) that would otherwise change  $V_{rest}$  and thereby confound the interpretation of a change in intracellular ion activity. Alternatively,  $V_m$  can be set to any desired value, or voltage steps can be applied to study voltage-dependent responses of intracellular ion activity. As shown in Fig. 2, this technique can be used to experimentally verify the settling time of the ISM and thereby define the high-frequency cutoff for reliably measuring  $V_{ion} = V_{ion-ISM} - V_{ref}$  when  $V_m$  is not constant.

Another advantage of the voltage-clamp configuration is the measurement of total membrane current,  $I_m$ , while simultaneously measuring intracellular ion activity. For example, the value of  $I_m$  needed to maintain any desired  $V_{hold}$  can be used as a criterion to ensure fiber viability after impalement of all the microelectrodes. Consequently,  $I_m$  also provides information about net ion flux, which can be combined with ISM measurement of ion activity to characterize membrane transport

systems. Here, we show that the combination of measuring dynamic changes of intracellular Na<sup>+</sup> activity and  $I_{pump}$  can be used to characterize the intracellular Na-dependence of the Na,K-ATPase in an intact skeletal muscle fiber (Fig. 5).

## Acknowledgments

We thank Dr. J.R. Lopez (Mount Sinai Medical Center) for kindly sharing his knowhow on the fabrication of liquid membrane ISMs.

This work was supported by the National Institute of Arthritis and Musculoskeletal and Skin Diseases, National Institutes of Health (R01-AR063710 to J.A. Heiny, R01-AR63182 to S.C. Cannon, and R21-AR067422 to M. DiFranco) and by the Muscular Dystrophy Association (MDA RG 381149 to S.C. Cannon).

The authors declare no competing financial interests.

Author contributions: The four-electrode technique and experimental studies were designed by J.A. Heiny, S.C. Cannon, and M. DiFranco. M. DiFranco performed the experiments; M. DiFranco and S.C. Cannon analyzed the data. J.A. Heiny, S.C. Cannon, and M. DiFranco wrote the paper.

Eduardo Ríos served as editor.

Submitted: 10 May 2019

Accepted: 18 June 2019

## References

- Aickin, C.C., and A.F. Brading. 1982. Measurement of intracellular chloride in guinea-pig vas deferens by ion analysis, 36chloride efflux and microelectrodes. *J. Physiol.* 326:139–154. <https://doi.org/10.1113/jphysiol.1982.sp014182>
- Aickin, C.C., W.J. Betz, and G.L. Harris. 1989. Intracellular chloride and the mechanism for its accumulation in rat lumbrical muscle. *J. Physiol.* 411: 437–455. <https://doi.org/10.1113/jphysiol.1989.sp017582>
- Ammann, D. 1986. *Ion-Selective Microelectrodes*. Springer-Verlag, Berlin. <https://doi.org/10.1007/978-3-642-52507-0>
- Armstrong, W.M., and J.F. Garcia-Diaz. 1980. Ion-selective microelectrodes: theory and technique. *Fed. Proc.* 39:2851–2859.
- Chen, T.W., T.J. Wardill, Y. Sun, S.R. Pulver, S.L. Renninger, A. Baohan, E.R. Schreiter, R.A. Kerr, M.B. Orger, V. Jayaraman, et al. 2013. Ultrasensitive fluorescent proteins for imaging neuronal activity. *Nature.* 499: 295–300. <https://doi.org/10.1038/nature12354>
- Davies, C.W. 1962. *Ion Association*. Butterworths, London.
- DiFranco, M., and J.L. Vergara. 2011. The Na conductance in the sarcolemma and the transverse tubular system membranes of mammalian skeletal muscle fibers. *J. Gen. Physiol.* 138:393–419. <https://doi.org/10.1085/jgp.20110682>
- DiFranco, M., A. Herrera, and J.L. Vergara. 2011. Chloride currents from the transverse tubular system in adult mammalian skeletal muscle fibers. *J. Gen. Physiol.* 137:21–41. <https://doi.org/10.1085/jgp.201010496>
- DiFranco, M., M. Quinonez, and J.L. Vergara. 2012. The delayed rectifier potassium conductance in the sarcolemma and the transverse tubular system membranes of mammalian skeletal muscle fibers. *J. Gen. Physiol.* 140:109–137. <https://doi.org/10.1085/jgp.201210802>
- DiFranco, M., H. Hakimjavadi, J.B. Lingrel, and J.A. Heiny. 2015a. Na,K-ATPase  $\alpha 2$  activity in mammalian skeletal muscle T-tubules is acutely stimulated by extracellular K<sup>+</sup>. *J. Gen. Physiol.* 146:281–294. <https://doi.org/10.1085/jgp.201511407>
- DiFranco, M., C. Yu, M. Quiñonez, and J.L. Vergara. 2015b. Inward rectifier potassium currents in mammalian skeletal muscle fibres. *J. Physiol.* 593: 1213–1238. <https://doi.org/10.1113/jphysiol.2014.283648>
- DiFranco, M., M. Quinonez, R. Dziedzic, A.M. Spokoiny, and S.C. Cannon. 2019. A highly-selective chloride microelectrode based on a mercuracarborand anion carrier. *bioRxiv*.
- Dulhunty, A.F. 1979. Distribution of potassium and chloride permeability over the surface and T-tubule membranes of mammalian skeletal muscle. *J. Membr. Biol.* 45:293–310. <https://doi.org/10.1007/BF01869290>
- Fu, Y., A. Struyk, V. Markin, and S. Cannon. 2011. Gating behaviour of sodium currents in adult mouse muscle recorded with an improved two-electrode voltage clamp. *J. Physiol.* 589:525–546. <https://doi.org/10.1113/jphysiol.2010.199430>
- Geukes Foppen, R.J. 2004. In skeletal muscle the relaxation of the resting membrane potential induced by K(+) permeability changes depends on Cl(-) transport. *Pflugers Arch.* 447:416–425. <https://doi.org/10.1007/s00424-003-1165-1>
- Kessler, M., L.C. Clark, D.W. Lubbers, and I.A. Silver. 1976. In: W. Simon, ed. *Ion and Enzyme Electrodes in Biology and Medicine*. Urban and Schwarzenberg, Munich, Germany.
- Kondo, Y., Y. Igarashi, K. Abe, and K. Tada. 1993. New double-barreled, ion-sensitive microelectrodes for measuring intracellular Cl<sup>-</sup> activities in rabbit renal collecting ducts. *Tohoku J. Exp. Med.* 169:51–58. <https://doi.org/10.1620/tjem.169.51>
- Koryta, J., and K. Stulik. 1983. *Ion-Selective Electrodes*. Cambridge University Press, Cambridge, London. <https://doi.org/10.1017/CBO9780511897610>
- Mooney, J.L., V. Lyall, M. Acevedo, and W.M. Armstrong. 1988. Double-barreled K<sup>+</sup>-selective microelectrodes based on dibenzo-18-crown-6. *Am. J. Physiol.* 255:C408–C412. <https://doi.org/10.1152/ajpcell.1988.255.3.C408>
- Pedersen, T.H., F.V. de Paoli, J.A. Flatman, and O.B. Nielsen. 2009. Regulation of ClC-1 and KATP channels in action potential-firing fast-twitch muscle fibers. *J. Gen. Physiol.* 134:309–322. <https://doi.org/10.1085/jgp.200910290>
- Tsien, R.Y. 1989. Fluorescent indicators of ion concentrations. *Methods Cell Biol.* 30:127–156. [https://doi.org/10.1016/S0091-679X\(08\)60978-4](https://doi.org/10.1016/S0091-679X(08)60978-4)
- Virkki, L.V., D.A. Wilson, R.D. Vaughan-Jones, and W.F. Boron. 2002. Functional characterization of human NBC4 as an electrogenic Na<sup>+</sup>-HCO cotransporter (NBCe2). *Am. J. Physiol. Cell Physiol.* 282:C1278–C1289. <https://doi.org/10.1152/ajpcell.00589.2001>
- Zeuthen, T., and C. Monge. 1975. Intra- and extracellular gradients of electrical potential and ion activities of the epithelial cells of the rabbit ileum in vivo recorded by microelectrodes. *Philos. Trans. R. Soc. Lond. B Biol. Sci.* 271:277–281. <https://doi.org/10.1098/rstb.1975.0052>